Metastable olivine wedge beneath the Japan Sea imaged by seismic interferometry

Zhichao Shen[1], and Zhongwen Zhan[1]

[1]Seismological Laboratory, California Institute of Technology, Pasadena, CA 91125, USA.

Corresponding author: Zhichao Shen (zshen@caltech.edu)

Key Points:

- We turn deep earthquakes into virtual receivers by inter-source interferometry, to detect metastable olivine wedge in subducted slab.
- We confirm the existence of the wedge about 30 km thick at 410-km depth and gradually diminishing to at least 610-km depth.
- Our results suggest the slab core in transition zone is dry and deep-focus earthquakes initiate by the phase change of olivine.

Abstract

The metastable olivine wedge (MOW) within subducted slabs has long been hypothesized to host deep-focus earthquakes (>300 km). Its presence would also rule out hydrous slabs being subducted into the mantle transition zone. However, the existence and dimensions of MOW remain controversial. Here, we apply inter-source interferometry, which converts deep earthquakes into virtual seismometers, to detect the seismic signature of MOW without influence from shallow heterogeneities. With data from the Hinet, we confirm the existence of MOW beneath the Japan Sea and constrain its geometry to be ~30 km thick at 410-km depth and gradually diminishing to a depth of 610 km at least. Our result supports transformational faulting of metastable olivine as the initiation mechanism of deep earthquakes, although large events (M7.0+) probably rupture beyond the wedge. Furthermore, the slab core must be dehydrated at shallower depth and only transports negligible amount of water into the transition zone.

1 Introduction

Global earthquakes mostly occur in the crust but can extent to ~700 km depth within subducting plates. Crustal earthquakes are thought to be driven by the brittle frictional failure (Scholz, 1998), while the nature of deep-focus earthquakes (depth >300 km) has been posed to geophysicists as a long-standing puzzle (Brace et al., 1980). Several mechanisms have been proposed for deep earthquakes, including the dehydration embrittlement (Meade & Jeanloz, 1991), thermal shear instability (Kanamori et al., 1998) and transformational faulting (Green et al., 1989). Among them, transformational faulting, which triggers the slip instability through a sudden phase change from metastable olivine to spinel, can naturally explain the depth dependent seismicity distribution that resurges in the transition zone with an abruptly cessation below 660 km (Houston, 2015). Moreover, recent laboratory experiments have shown fracture nucleation and later intense acoustic emissions associated with the olivine-to-spinel phase transformation (Schubnel et al., 2013, Wang et al., 2017), thus making the transformational faulting hypothesis more appealing.

For transformational faulting to happen, it is hypothesized that the low-pressure polymorphs of olivine inside cold slabs could metastably extend into the mantle transition zone (MTZ), forming a tongue-shaped “Metastable Olivine Wedge” (MOW). Furthermore, the positively buoyant MOW, if present, may slow down the subducting slab in the MTZ (Bina et al., 2001), or even resist the slab from penetrating into the lower mantle (Tetzlaff & Schmeling, 2000).

The dimension of MOW is generally thought to correlate with the slab thermal parameter (Kirby et al., 1996), but the water content of subducted slab and the latent heat due to the phase changes also play crucial roles (Mosenfelder et al., 2001, Frane et al., 2013). Laboratory experiments demonstrated that incorporation of a small amount of H_2O leads to a remarkable boost in the olivine to ringwoodite transformation rate via hydrolytic weakening process (Frane et al., 2013). The latent heat feedback together with an additional intracrystalline transformation mechanism significantly reduces the maximum depth that MOW can reach as suggested from an updated thermo-kinetic model (Monsenfelder et al., 2001). Therefore, the existence and exact geometry of MOW would provide essential constraints on the thermal-petrological properties of subducting slabs.

However, seismic imaging of the low-velocity MOW structure has been particularly challenging. For instance, body wave travel-time analysis ubiquitously suffers from the wavefront healing effect. A thermal slab without MOW could satisfactorily predict high-resolution seismic arrival times, but the inclusion of MOW merely offers a subtle improvement on the data fitting (Koper et al., 1998) It has also been illustrated that the metastable olivine can be unveiled from waveform distortions of some seismic phases that travel through it (Vidale et al., 1991, Koper & Wiens, 2000). Nonetheless, deterministically examining the seismogram involves onerous effort because lithospheric heterogeneities contribute great complexities on the seismogram and smear the illumination of deep slab. Given the difficulty in resolving MOW, its thicknesses reported from preceding studies differ by 50 km at the 410-km discontinuity in Japan subduction zone (Lidaka & Suetsugu, 1992; Jiang & Zhao, 2011; Kawakatsu & Yoshioka, 2011; Furumura et al., 2016) (Table S1), leaving the metastable persistence of olivine and its detail geometry hitherto ambiguous.

2 Inter-source interferometry

To untangle the potentially subtle seismic signature of metastable olivine from complex shallow Earth heterogeneities, we apply inter-source interferometry (Curtis et al., 2009; Tonegawa & Nishida, 2010) to deep earthquake pairs in the Japan subduction zone (Figure 1a). For conventional inter-receiver interferometry, cross-correlations of diffusive earthquake coda or ambient noise field reconstruct Green's functions between receiver pairs (Campillo & Paul, 2003). Equivalently, due to reciprocity, by cross-correlating coda waves from an earthquake pair, the inter-source interferometry synthesizes the transient strain triggered by passing seismic waves from one source to the other. This is as if we convert one of the deep earthquakes to a virtual seismometer deployed below the complex shallow layers and record the other event. To avoid violating the impulsive-source condition in reciprocity, we select five deep-focus earthquakes of small magnitudes (4.0≤Mw≤5.2) with simple source process (<10% non-double-couple component). Among them, three earthquakes (S1, S2, S3) are refined at ~360 km depth whereas the other two (D1, D2) are at depths of ~580 km (Figure S1 and S2; see Supplementary for relocation details), corresponding to the shallow and deep ends of hypothesized MOW respectively. Although receivers in the inter-source interferometry should have a complete azimuthal coverage, the stationary phase approximation greatly loosens the receiver geometry restriction (Snieder, 2004). For our targeted slab beneath the Japan Sea, Hi-net stations situate around the stationary phase region of the deep earthquake pairs (Figure 1b), hereby providing an ideal source-receiver configuration to isolate the deep slab structures from other complexities.

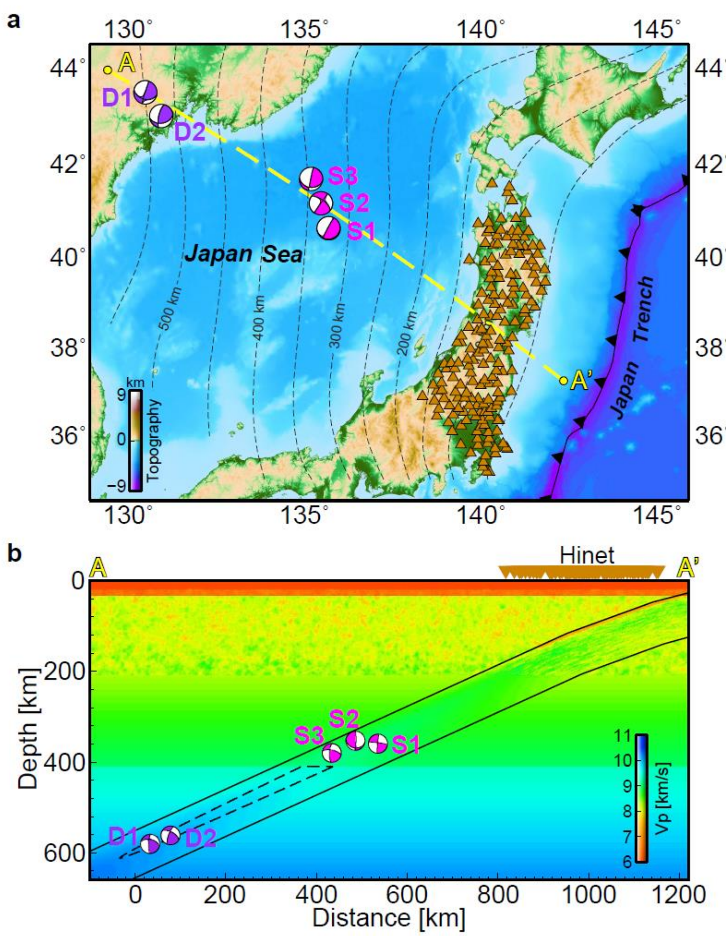

Figure 1. Map view of our targeted area and depth profile of Japan subduction zone. (a). Map of this study area. Black dashed lines are the slab depth contours from Slab2.0 model (Hayes et al., 2018). Orange triangles are Hi-net stations used in our interferometry. The purple and magenta beachballs are from Japan Meteorological Agency and represent the earthquake depths of ~580 km (D1, D2) and ~360 km (S1, S2, S3), respectively. (b). P-wave velocity profile derived from thermal modeling along AA'. The black solid line and black dashed line represent the geometry of subducting Pacific slab and hypothesized MOW respectively. Above 200 km depth, small scale heterogeneities are included. D1/D2 and S1/S2/S3 correspond to the deep (~580 km) and shallow (~360 km) end of the MOW respectively.

We first validate the inter-source interferometry method for two synthetic scenarios with and without MOW. The velocity and density profiles of slab and MOW are constructed based on a thermal model tuned for the Japan subduction zone (see Supplementary for modeling details). Small-scale heterogeneities are implemented at shallow depths to produce realistic coda waves (Figure 1b; Furumura & Kennett, 2005). Given the velocity and density profiles, we simulated the elastic wavefield with a GPU-based 2D finite difference code in Cartesian coordinates, which is eighth-order in space and second-order in time (Li et al., 2014). With a minimum shear velocity of 2.8 km/s, a grid spacing of 75 m and time step of 0.001s, our computed synthetic waveforms are accurate up to 6 Hz with sampling of at least six grids per wavelength. After computing synthetic seismograms on the surface from deep earthquakes D1 and S1, we filter and cut the vertical-component coda waves from 5 s to 45 s after the P wave first arrivals for interferometry. The 40-s long window is further cut into 10-s long overlapping segments offset by 2 s. The cross-correlations of all the segments are then normalized by the maximum and averaged to account for the coda energy decay with time. For the D1-S1 earthquake pair in both scenarios, the 0.2~2 Hz cross-correlation record section presents coherent waveforms with constant arrival time across the profile of Hi-net (Figure S3). This indicates that our simulated coda wavefields are diffuse due to shallow heterogeneities and the inter-source Green's function could be extracted by coda interferometry at a single station (Snieder, 2004). To enhance the coherent signal, we stack the cross-correlations over all the stations. In both scenarios with and without MOW, the resulting interferometric waveforms match the directly simulated P-wave strain seismograms from source D1 to virtual receiver S1, and meanwhile, capture the polarity flip (Figure S3b vs. S3c) caused by the P-wave interaction with the MOW (Figure S4). Since absolute arrival times have strong trade-offs with earthquake locations, herein we focus solely on interpreting the waveform shape.

3 Results

Having shown the feasibility to retrieve the P-wave strain Green's functions between two deep earthquakes, we apply the inter-source interferometry method to real data on the Hi-net stations (Figure 1). As an example, the cross-correlation record section for the D1-S1 earthquake pair at 0.2~2 Hz exhibits coherent signals arriving at a constant time in a wide azimuth range (Figure 2a), implying a diffuse coda wavefield. The stacked waveform presents a negative trough preceding a positive peak, similar to that of aforementioned synthetic case with a MOW (Figure 2c). Furthermore, the interferometric results of the other five earthquake pairs from D1/D2 to S1/S2/S3 are in good agreement with that of D1-S1 pair (Figure S5), all favoring a MOW structure. Beside the MOW cause, we also scrutinize other alternatives that could result in the negative pulse, such as opposite focal mechanisms and a low-velocity hydrous oceanic crust on top of the slab. First motion analysis shows that the Hi-net stations used for interferometry share same P wave polarities for all the selected deep earthquakes (Figure 2b and S6), so radiation patterns alone can not explain the negative polarities of the correlations. An 8 km thick oceanic crust with a velocity reduction of 8% extending to 660 km fails to reproduce our observations as well (Figure 2c and S7). With these alternative possibilities ruled out, we suggest the existence of metastable olivine beneath the Japan Sea as the preferred interpretation.

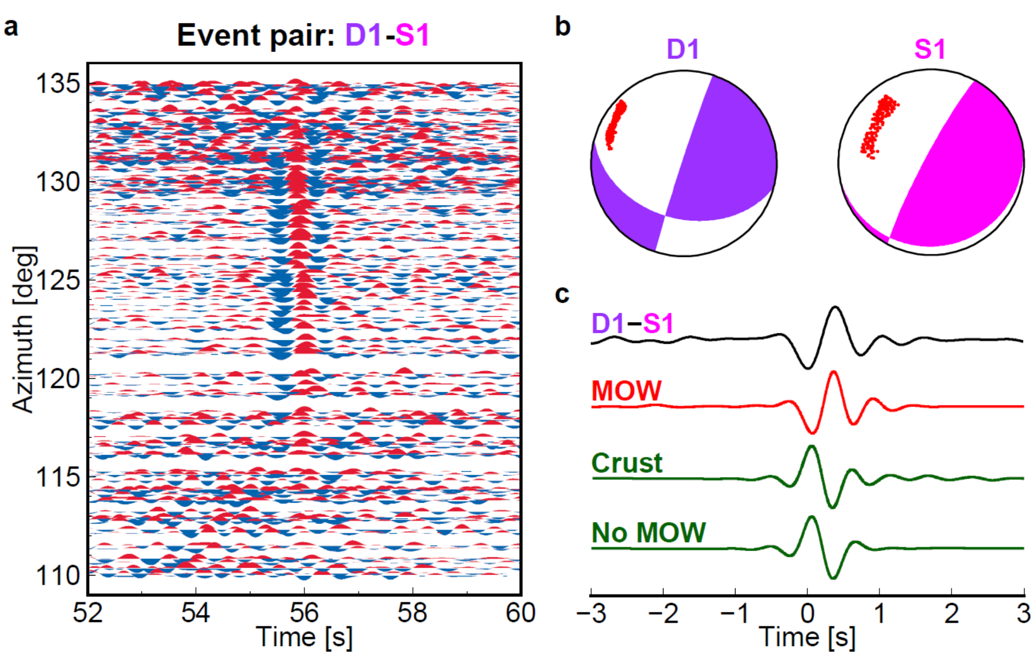

Figure 2. Inter-source interferometry results at 0.2~2 Hz suggest the existence of metastable olivine beneath the Japan Sea. (a). The record section of coda wave cross-correlations as a function

of azimuth for the D1-S1 earthquake pair. Blue and red color correspond to the negative and positive phases respectively. Coherent signals with negative polarities arrive at a constant time across Hi-net stations. (b). First motion analysis for deep earthquake D1 and S1. At Hi-net stations (red dots), both events share the same P-wave polarities. (c). Waveform comparison of observations and synthetics. The top black trace is the stacked cross-correlation waveform for D1-S1 deep earthquake pair in (a). The red and dark green lines are the synthetic strain waveforms for cases of a thermal slab with MOW (MOW), a thermal slab with hydrous oceanic crust (Crust) and a thermal slab only (No MOW), respectively. All the traces are aligned by their peak phases. Only the MOW model predicts the waveform shape observed in D1-S1 pair.

To better quantify the MOW dimension and depth extent, which are both important for understanding deep earthquake physics and slab hydrous state, we need to appeal to higher frequency interferometric waveforms. For example, we show that the 0.2~2 Hz cross-correlation waveforms are insensitive to the location of S1/S2/S3 relative to the MOW (Figure S8), which in turn provide little information on the thickness of MOW at the shallow end. On the other hand, at 0.2~5 Hz, synthetic strains are significantly distorted across a short distance range (Figure S8). Hence, with well-constrained relative locations among the virtual sensors S1, S2, and S3, we can use higher frequency (up to 5 Hz) waveform details at different locations to determine the geometry of metastable olivine. Indeed, for synthetic tests with a set of earthquake pairs, the inter-source interferometry is shown to be capable of extracting 5 Hz transient strains and capturing the waveform variations at different virtual sensors (Figure S9).

Subsequently with the real data from Hi-net, we retrieve the 0.2~5 Hz strain responses for all six earthquake pairs from D1/D2 to S1/S2/S3 following the same interferometry procedures (Figure S10). Taking D1 as an example, virtual sensor S1 records a simple trace with negative polarity, but the other two (S2 and S3) present splitting waveforms that consist of two phases (Figure 3c). To evaluate the robustness of observed waveform complexity, we estimated the 95% confidence intervals for stacked cross-correlations using a bootstrapping technique. All the coherent signals evidently stand above the noise level with narrow uncertainties, and the traces characterized by splitting phases are unlikely to be caused by noise (Figure S11). The distinct interferometric waveforms appear to correlate with the spatial distribution of virtual sensors: S2 and S3 with splitting phases are close to the slab upper interface whereas S1 with a single phase sits near the slab core (Figure 3a). In addition, similar interferometric results from the other deep earthquake D2, though with slightly higher noise levels, suggest our 0.2-5 Hz correlations converge to robust waveforms (Figure S11).

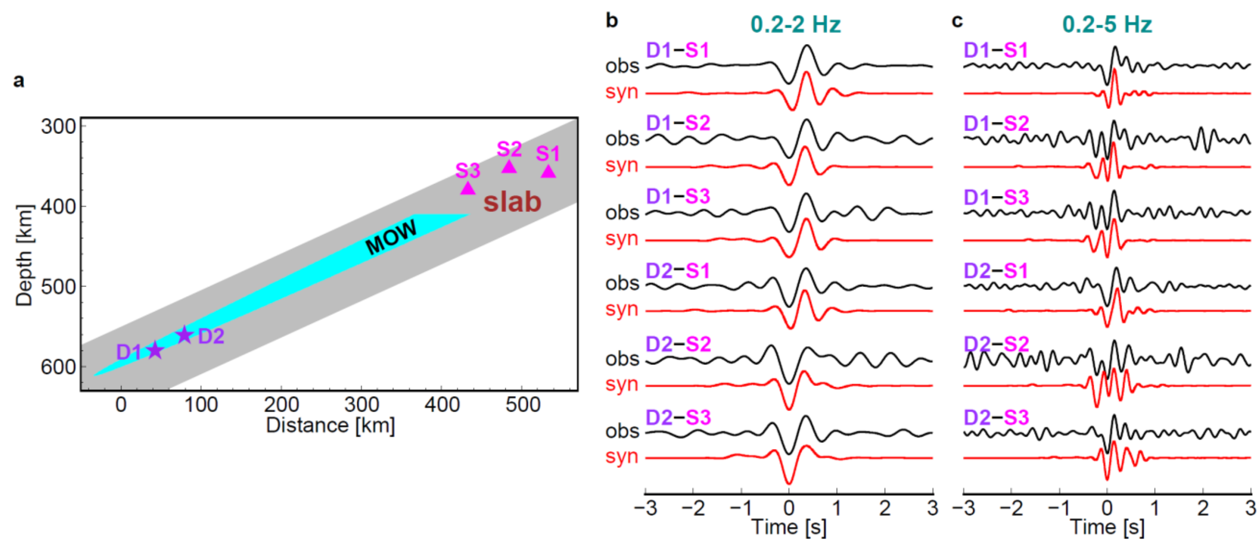

Figure 3. Proposed MOW dimension can reproduce our inter-source interferometry observations. (a) Slab profile with deep earthquakes D1/D2 and three virtual receivers (S1-S3). The gray and cyan region denote the slab and our proposed MOW respectively. The P-wave velocity within MOW decreases 5%. Both D1 and D2 need to be within MOW to explain the interferometric waveforms. (b). 0.2~2 Hz waveform comparison of inter-source interferometric observations (black lines) and synthetics (red lines) for all deep earthquake pairs. (c). similar to (b) but for higher frequency up to ~5 Hz. All six waveforms are well fitted by our suggested MOW model.

To account for these high frequency waveform variations, we grid-searched a variety of MOW geometries through physics-based modeling. Assuming that temperature is the first order control on the olivine phase transformation, the MOW would thus be defined as the region colder than a kinetic cut-off temperature (T_{mow}) in our initial thermal slab. In searching for the optimal MOW geometry to fit our interferometric observations, we directly computed the synthetic waveforms at virtual seismometer S1/S2/S3 from deep earthquake D1/D2. When comparing the synthetics with observations, we tested different kinetic kick-off temperatures as well as the deep earthquake locations relative to MOW allowing a maximum arrival time difference of 1.5 s. We found that both 0.2~2 Hz and 0.2~5 Hz interferometric waveforms can be adequately fitted when T_{mow} is defined as 664 ℃ with D1 situating at the lower boundary of metastable olivine (Figure 3). The resolved P-wave velocity within MOW is 4%~5% lower than the surrounding slab velocity (2%~3% lower than that of ambient mantle; Figure S12), which is consistent with previous studies (Jiang & Zhao, 2011; Furumura et al., 2016). As an independent argument, the same MOW model does also provide a good fit to interferometric observations at the three virtual receivers from the other deep earthquake D2 (Figure 3). Despite that the 5-Hz interferometric waveform details are not fully explained due to lateral variations in slab structures, the observed waveform features (polarities, single or splitting phases) are generally retained in synthetic seismograms. Here, we emphasize that our new interferometry observations constrain the MOW geometry and velocity reduction, instead of the cut-off temperature (T_{mow}) or the thermal model. For scenarios with different combinations of slab parameters (e.g., subduction rate, age), T_{mow} that fits the data best can vary by tens of degrees (Figure S13). Nonetheless, the MOW structures consistently resemble a thickness of ~30 km across the slab at 410 km and gradually diminish to a depth of ~610 km at least.

4 Discussion and Conclusions

Compared to previously proposed MOW geometries in nearby regions, our MOW at 410 km depth is slightly thicker than that imaged by the receiver function (Kawakatsu & Yoshioka, 2011), but considerably thinner than that derived from traveltime based studies (Table S1). With our resolved MOW dimension, the delay of olivine phase transformation is estimated to increase the slab buoyancy by 1% below 410 km, which is comparable to the thermal slab buoyancy force (2~3%; Cammarano et al., 2003). Such extra buoyancy force generated by the metastable olivine could in turn reduce the slab subduction rate (Tetzlaff & Schmeling, 2000). Given the age of Japan trench (Sdrolias & Müller, 2006), the associated metastable olivine for a 130 Ma oceanic lithosphere is estimated to slow down the subduction rate by up to ~12% (Bina et al., 2001). For colder slabs, such as Tonga, the effect might be even stronger, due to the presumably larger metastable olivine wedge. In our preferred scenario (Figure 4), deep earthquakes D1 and D2 occur within MOW, supporting transformational faulting as the cause of deep earthquakes. Assuming a circular crack and a constant strain drop (Vallee, 2013), the metastable olivine thickness (~7 km) at 600 km depth is equivalent to the dimension of a moderate magnitude earthquake (Mw6~7) that ruptures across the slab. To host larger deep earthquakes (e.g. Mw7+) with larger rupture dimensions, which did occur beneath the Japan Sea and in other warmer subduction zones with potentially thinner MOWs, the slip instability probably nucleates within MOW by transformational faulting and later propagate outside driven by other mechanisms (e.g., the thermal shear instability). The switch of mechanism around M6~7 would break the self-similarity of deep earthquake sizes and cause a change in the Gutenberg-Richter distributions (i.e., b values), which is recently observed (Zhan, 2017). Furthermore, models of great deep earthquakes, such as the 1994 Mw8.2 Bolivia earthquake and the 2018 Mw8.0 Fiji-Tonga doublet, also imply two-stage rupture processes and exemplify local slab temperature as the critical factor for deep earthquakes (Zhan et al., 2014).

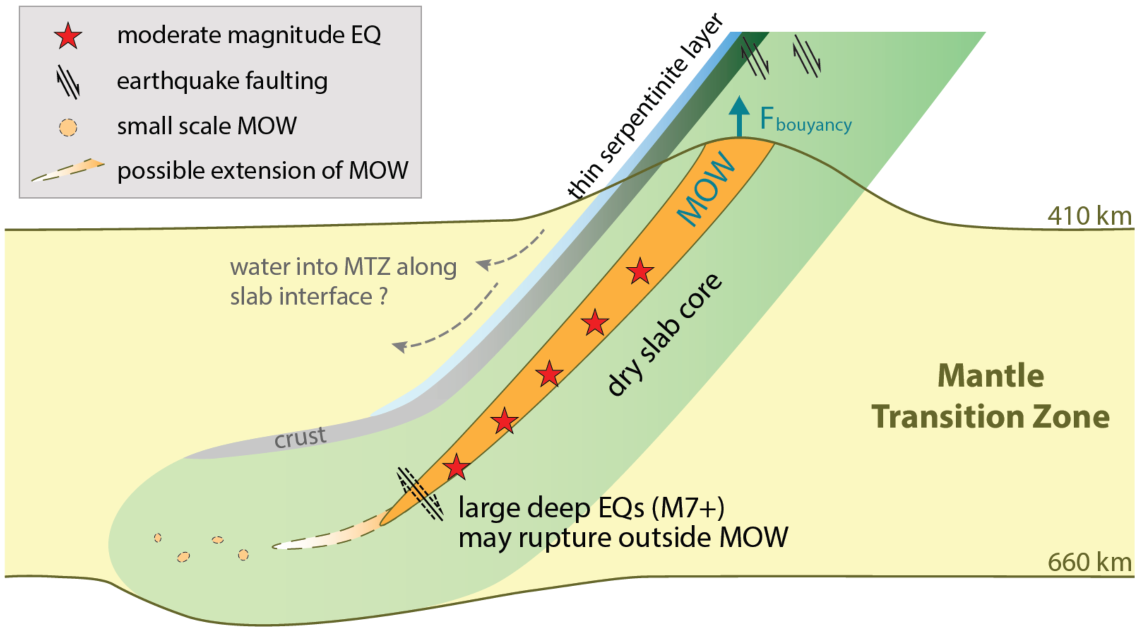

Figure 4. Schematic cross-section of subducted slab in the mantle transition zone. Metastable olivine persists in the slab core as a wedge extending down to the bottom of MTZ. The red stars indicate moderate magnitude EQs. Deep earthquakes can initiate within MOW by transformational faulting, but larger deep earthquakes (black dashed faulting) may potentially rupture outside MOW driven by other mechanisms. The existence of MOW requires that the core of subducted slab must carries negligible amount of water. But it is still possible that the water can be transported into the mantle transition zone along the slab interface.

The depth extent of our proposed MOW indicates an extremely dry Pacific slab core (<75 wt ppm) in the MTZ beneath the Japan Sea (Figure 4; Kawakatsu & Yoshioka, 2011; Frane et al., 2013). However, the arc volcanism, intermediate-depth earthquakes, and high-resolution tomography models all point to substantially hydrated slab above 200 km depth (Hasegawa & Nakajima, 2017; Cai et al., 2018), potentially through outer-rise plate-bending faults that cut deep into the incoming plate as pathways for water (Ranero et al., 2003). Therefore, the water associated with these faults must be expelled almost completely into the mantle at intermediate depths (Kawakatsu & Watada, 2007), carrying negligible amount of water into the MTZ (Green et al., 2010). Conversely, garnering evidences from ultradeep diamond inclusions (Pearson et al., 2014), mineral experiments (Kohlstedt et al., 1996) and electromagnetic induction data (Kelbert et al., 2009) have demonstrated that the MTZ can, at least locally, harbor substantial amount of water (up to ~2.5

wt%). Given the distance between our MOW and plate interface (~24 km) and the hydrogen diffusion coefficients of olivine and its polymorphs (Hae et al., 2006), it is still possible that a thin layer near the subducting plate provide potential pathways for transporting water into MTZ, such as a narrow serpentinite channel on top of the slab (Kawakatsu & Watada, 2007). Or instead of linking to current subduction, the water reservoir in MTZ might be associated with other tectonic processes including the delamination of hydrous mantle lithosphere (Green et al., 2010) or rising of hydrous magmas (Hirschmann, 2006).

Acknowledgments

We are grateful to Micheal Gurnis, Paul Asimow, Sidao Ni and Wenbo Wu for discussions and suggestions. Seismic data are collected from the Data Management Center of the Incorporated Research Institutions for Seismology (https://www.iris.edu/dms/nodes/dmc), Hi-net (http://www.hinet.bosai.go.jp/) and F-net (http://www.fnet.bosai.go.jp/). The earthquake catalog and focal mechanisms are downloaded from ISC-EHB distributed by the International Seismological Centre (ISC, http://www.isc.ac.uk/) and National Research Institute for Earth Science and Disaster Resilience (NIED, http://www.fnet.bosai.go.jp/event/search.php?LANG=en). The earthquake arrival time data is available at the Japan Meteorological Agency (JMA, http://www.data.jma.go.jp/svd/eqev/data/bulletin/index_e.html).

References

Bina, C. R., Stein, S., Marton, F. C., & Van Ark, E. M. (2001). Implications of slab mineralogy for subduction dynamics. *Physics of the Earth and Planetary Interiors*, 127(1-4), 51-66.

Brace, W. F., & Kohlstedt, D. L. (1980). Limits on lithospheric stress imposed by laboratory experiments. *Journal of Geophysical Research: Solid Earth*, 85(B11), 6248-6252.

Cai, C., Wiens, D. A., Shen, W., & Eimer, M. (2018). Water input into the Mariana subduction zone estimated from ocean-bottom seismic data. *Nature*, 563(7731), 389.

Cammarano, F., Goes, S., Vacher, P., & Giardini, D. (2003). Inferring upper-mantle temperatures from seismic velocities. *Physics of the Earth and Planetary Interiors*, 138(3-4), 197-222.

Campillo, M., & Paul, A. (2003). Long-range correlations in the diffuse seismic coda. *Science*, 299(5606), 547-549.

Curtis, A., Nicolson, H., Halliday, D., Trampert, J., & Baptie, B. (2009). Virtual seismometers in the subsurface of the Earth from seismic interferometry. *Nature Geoscience*, 2(10), 700.

Du Frane, W. L., Sharp, T. G., Mosenfelder, J. L., & Leinenweber, K. (2013). Ringwoodite growth rates from olivine with∼ 75 ppmw H_2O: metastable olivine must be nearly anhydrous to exist in the mantle transition zone. *Physics of the Earth and Planetary Interiors*, 219, 1-10.

Furumura, T., & Kennett, B. L. N. (2005). Subduction zone guided waves and the heterogeneity structure of the subducted plate: Intensity anomalies in northern Japan. *Journal of Geophysical Research: Solid Earth*, 110(B10).

Furumura, T., Kennett, B. L., & Padhy, S. (2016). Enhanced waveguide effect for deep-focus earthquakes in the subducting Pacific slab produced by a metastable olivine wedge. *Journal of Geophysical Research: Solid Earth*, 121(9), 6779-6796.

Green II, H. W., & Burnley, P. C. (1989). A new self-organizing mechanism for deep-focus earthquakes. *Nature*, 341(6244), 733.

Green II, H. W., Chen, W. P., & Brudzinski, M. R. (2010). Seismic evidence of negligible water carried below 400-km depth in subducting lithosphere. *Nature*, 467(7317), 828.

Hae, R., Ohtani, E., Kubo, T., Koyama, T., & Utada, H. (2006). Hydrogen diffusivity in wadsleyite and water distribution in the mantle transition zone. *Earth and Planetary Science Letters*, 243(1-2), 141-148.

Hasegawa, A., & Nakajima, J. (2017). Seismic imaging of slab metamorphism and genesis of intermediate-depth intraslab earthquakes. *Progress in Earth and Planetary Science*, 4(1), 12.

Hayes, G. P., Moore, G. L., Portner, D. E., Hearne, M., Flamme, H., Furtney, M., & Smoczyk, G. M. (2018). Slab2, a comprehensive subduction zone geometry model. *Science*, 362(6410), 58-61.

Hirschmann, M. M. (2006). Water, melting, and the deep Earth H_2O cycle. *Annu. Rev. Earth Planet. Sci.*, 34, 629-653.

Houston, H. (2015). 4.13—deep earthquakes. In G. Schubert (Ed.), *Treatise on geophysics* (2nd ed., pp. 329–354). Oxford: Elsevier.https://doi.org/10.1016/B978-0-444-53802-4.00079-8

Jiang, G., & Zhao, D. (2011). Metastable olivine wedge in the subducting Pacific slab and its relation to deep earthquakes. *Journal of Asian Earth Sciences*, 42(6), 1411-1423.

Jiang, G., Zhao, D., & Zhang, G. (2008). Seismic evidence for a metastable olivine wedge in the subducting Pacific slab under Japan Sea. *Earth and Planetary Science Letters*, 270(3-4), 300-307.

Jiang, G., Zhao, D., & Zhang, G. (2015). Detection of metastable olivine wedge in the western Pacific slab and its geodynamic implications. *Physics of the Earth and Planetary Interiors*, 238, 1-7.

Kanamori, H., Anderson, D. L., & Heaton, T. H. (1998). Frictional melting during the rupture of the 1994 Bolivian earthquake. *Science*, 279(5352), 839-842.

Kaneshima, S., Okamoto, T., & Takenaka, H. (2007). Evidence for a metastable olivine wedge inside the subducted Mariana slab. *Earth and Planetary Science Letters*, 258(1-2), 219-227.

Kawakatsu, H., & Watada, S. (2007). Seismic evidence for deep-water transportation in the mantle. *Science*, 316(5830), 1468-1471.

Kawakatsu, H., & Yoshioka, S. (2011). Metastable olivine wedge and deep dry cold slab beneath southwest Japan. *Earth and Planetary Science Letters*, 303(1-2), 1-10.

Kelbert, A., Schultz, A., & Egbert, G. (2009). Global electromagnetic induction constraints on transition-zone water content variations. *Nature*, 460(7258), 1003.

Kennett, B. L. N., & Engdahl, E. R. (1991). Traveltimes for global earthquake location and phase identification. *Geophysical Journal International*, 105(2), 429-465.

Kirby, S. H., Stein, S., Okal, E. A., & Rubie, D. C. (1996). Metastable mantle phase transformations and deep earthquakes in subducting oceanic lithosphere. *Reviews of geophysics*, 34(2), 261-306.

Kohlstedt, D. L., Keppler, H., & Rubie, D. C. (1996). Solubility of water in the α, β and γ phases of $(Mg, Fe)_2SiO_4$. *Contributions to Mineralogy and Petrology*, 123(4), 345-357.

Koper, K. D., & Wiens, D. A. (2000). The waveguide effect of metastable olivine in slabs. *Geophysical Research Letters*, 27(4), 581-584.

Koper, K. D., Wiens, D. A., Dorman, L. M., Hildebrand, J. A., & Webb, S. C. (1998). Modeling the Tonga slab: Can travel time data resolve a metastable olivine wedge? *Journal of Geophysical Research: Solid Earth*, 103(B12), 30079-30100.

Laske, G., Masters, G., Ma, Z., & Pasyanos, M. (2013, April). Update on CRUST1. 0—A 1-degree global model of Earth's crust. In *Geophys. Res. Abstr* (Vol. 15, p. 2658). Vienna, Austria: EGU General Assembly.

Li, D., Helmberger, D., Clayton, R. W., & Sun, D. (2014). Global synthetic seismograms using a 2-D finite-difference method. *Geophysical Journal International*, 197(2), 1166-1183.

Lidaka, T., & Furukawa, Y. (1994). Double seismic zone for deep earthquakes in the Izu-Bonin subduction zone. *Science*, 263(5150), 1116-1118.

Lidaka, T., & Suetsugu, D. (1992). Seismological evidence for metastable olivine inside a subducting slab. *Nature*, 356(6370), 593.

Meade, C., & Jeanloz, R. (1991). Deep-focus earthquakes and recycling of water into the Earth's mantle. *Science*, 252(5002), 68-72.

Mosenfelder, J. L., Marton, F. C., Ross II, C. R., Kerschhofer, L., & Rubie, D. C. (2001). Experimental constraints on the depth of olivine metastability in subducting lithosphere. *Physics of the Earth and Planetary Interiors*, 127(1-4), 165-180.

Moresi, L., Quenette, S., Lemiale, V., Meriaux, C., Appelbe, B., & Mühlhaus, H. B. (2007). Computational approaches to studying non-linear dynamics of the crust and mantle. *Physics of the Earth and Planetary Interiors*, 163(1-4), 69-82.

Okada, Y., Kasahara, K., Hori, S., Obara, K., Sekiguchi, S., Fujiwara, H., & Yamamoto, A. (2004). Recent progress of seismic observation networks in Japan—Hi-net, F-net, K-NET and KiK-net—. *Earth, Planets and Space*, 56(8), xv-xxviii.

Pearson, D. G., Brenker, F. E., Nestola, F., McNeill, J., Nasdala, L., Hutchison, M. T., Matveev, S. et al. (2014). Hydrous mantle transition zone indicated by ringwoodite included within diamond. *Nature*, 507(7491), 221.

Ranero, C. R., Morgan, J. P., McIntosh, K., & Reichert, C. (2003). Bending-related faulting and mantle serpentinization at the Middle America trench. *Nature*, 425(6956), 367.

Sato, H., Fehler, M. C., & Maeda, T. (2012). *Seismic wave propagation and scattering in the heterogeneous earth* (Vol. 496). Berlin: Springer.

Schubnel, A., Brunet, F., Hilairet, N., Gasc, J., Wang, Y., & Green, H. W. (2013). Deep-focus earthquake analogs recorded at high pressure and temperature in the laboratory. *Science*, 341(6152), 1377-1380.

Scholz, C. H. (1998). Earthquakes and friction laws. *Nature*, 391(6662), 37.

Sdrolias, M., & Müller, R. D. (2006). Controls on back-arc basin formation. *Geochemistry, Geophysics, Geosystems*, 7(4).

Snieder, R. (2004). Extracting the Green's function from the correlation of coda waves: A derivation based on stationary phase. *Physical Review E*, 69(4), 046610.

Tetzlaff, M., & Schmeling, H. (2000). The influence of olivine metastability on deep subduction of oceanic lithosphere. *Physics of the Earth and Planetary Interiors*, 120(1-2), 29-38.

Tonegawa, T., & Nishida, K. (2010). Inter-source body wave propagations derived from seismic interferometry. *Geophysical Journal International*, 183(2), 861-868.

Turcotte, D., & Schubert, G. (2014). *Geodynamics*. Cambridge university press.

Vallée, M. (2013). Source time function properties indicate a strain drop independent of earthquake depth and magnitude. *Nature communications*, 4, 2606.

Vidale, J. E., Williams, Q., & Houston, H. (1991). Waveform effects of a metastable olivine tongue in subducting slabs. *Geophysical Research Letters*, 18(12), 2201-2204.

Wang, Y., Zhu, L., Shi, F., Schubnel, A., Hilairet, N., Yu, T., ... & Li, Z. (2017). A laboratory nanoseismological study on deep-focus earthquake micromechanics. *Science advances*, 3(7), e1601896.

Wiens, D. A., McGuire, J. J., & Shore, P. J. (1993). Evidence for transformational faulting from a deep double seismic zone in Tonga. *Nature*, 364(6440), 790.

Zhan, Z. (2017). Gutenberg–Richter law for deep earthquakes revisited: A dual-mechanism hypothesis. *Earth and Planetary Science Letters*, 461, 1-7.

Zhan, Z., Helmberger, D. V., & Li, D. (2014). Imaging subducted slab structure beneath the Sea of Okhotsk with teleseismic waveforms. *Physics of the Earth and Planetary Interiors*, 232, 30-35.

Zhan, Z., Kanamori, H., Tsai, V. C., Helmberger, D. V., & Wei, S. (2014). Rupture complexity of the 1994 Bolivia and 2013 Sea of Okhotsk deep earthquakes. *Earth and Planetary Science Letters*, 385, 89-96.